SUPPLEMENTARY NOTE

Mutation signature analysis

Mutational signatures are defined as patterns in the occurrence of somatic single-nucleotide variants that can reflect underlying mutational and DNA repair processes. We used non-negative matrix factorization (NMF) and principal component analysis (PCA) to define mutation signatures, and then estimated their contribution to each sample's mutational spectrum using somaticSignature R package. P-values for respective cohorts were calculated by way of Mann Whitney U tests. COSMIC mutational signatures were obtained from the COSMIC: Catalogue of Somatic Mutations in Cancer (http://cancer.sanger.ac.uk/cosmic), and were based on published report **(Online Methods)**.

We observed that the major differences between the nuclear core and periphery in mutational signatures also persisted even when we adjusted for both chromatin and replication timing. In the SKCA cohort, there was a proportionally higher burden of UV-mediated DNA damage and trans-lesion synthesis errors in the pyrimidine dimer context in the nuclear periphery relative to that in the core, even when controlling for replication timing and chromatin. cLADs also had a larger contribution of the mutational signature SSKCA1, dominated by T[C>T]W substitutions, while iLADs had a relative enrichment of mutational signature SSKCA2, representing C[C>T]Y; these preferences were observed even after adjusting for both chromatin and replication timing. The preference for C[C>T]N (where N: A, T, G, or C) in iLADs over cLADs was detectable in other cancer types including LUSC. Moreover, in the LUSC cohort, the signature of oxidative DNA damage marked by C>A substitutions, especially W[C>A]W, was more common in the cLADs even after adjusting for chromatin and replication timing (Mann Whitney U test p-value<1e-10). The increased incidence of somatic mutations in the WNW context was also detected across most cancer types regardless of replication timing and chromatin context. In the DLBCL and CLL cohorts, we observed an increase in C>T transitions in iLADs and an increase in T>G transversions in the WTN tri-nucleotide context in cLADs (Mann Whitney U test p-value<1e-05).

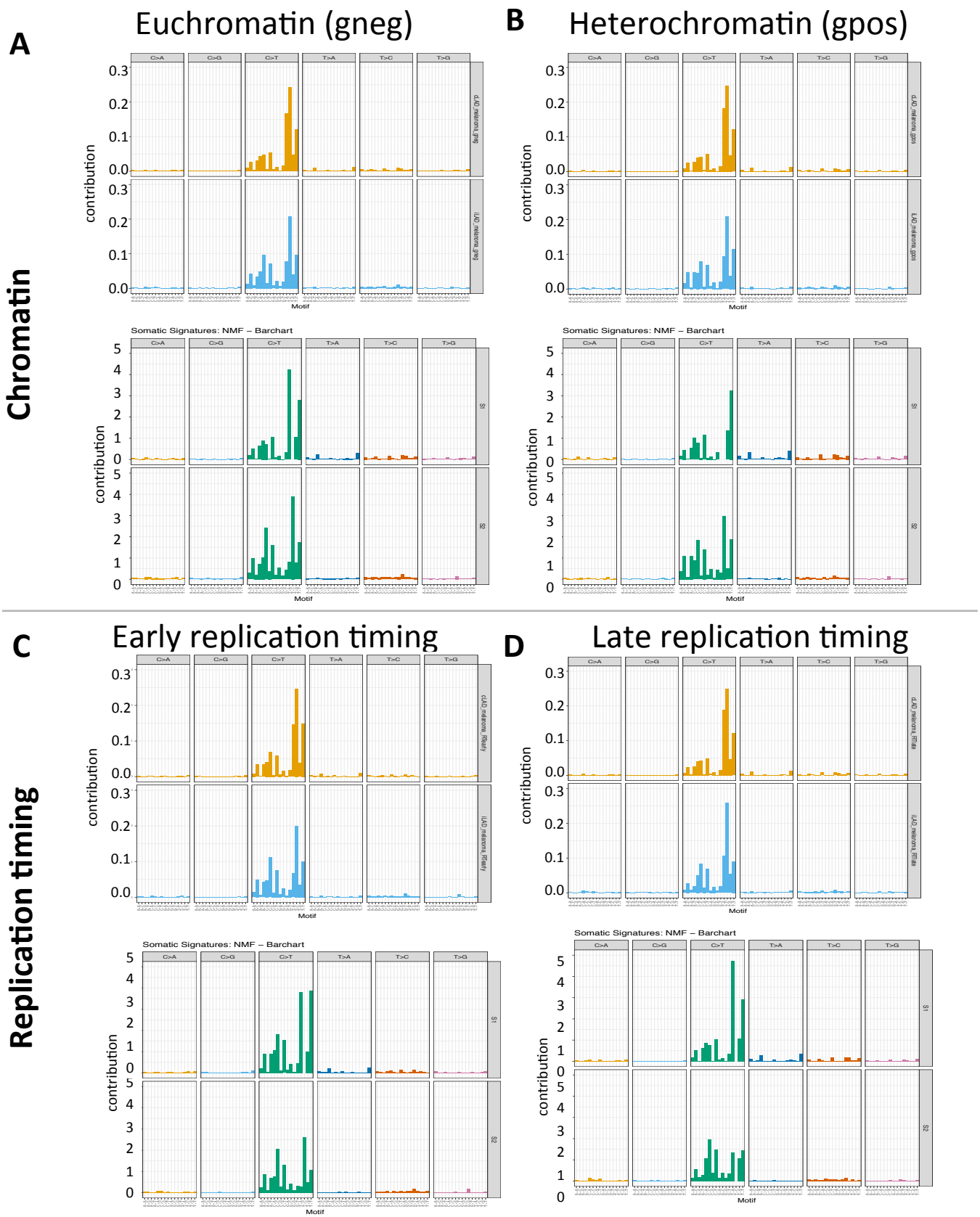

Comparing mutation signatures between nuclear core and periphery after adjusting for covariates in SKCA cohort. Somatic substitution patterns in their tri-nucleotide context (x-axis) and contribution (y-axis) of those substitution classes to the major mutation signatures in A) euchromatic (Giemsa-negative), B) heterochromatic (Giemsa-positive), C) constant early replicating, and D) constant late replication timing regions in the SKCA cohort. Order of the tri-nucleotide context is similar to that in Supplementary Figure 5. Plots were generated with the SomaticSignatures R package. Certain mutation signatures show variation depending on the nuclear context.

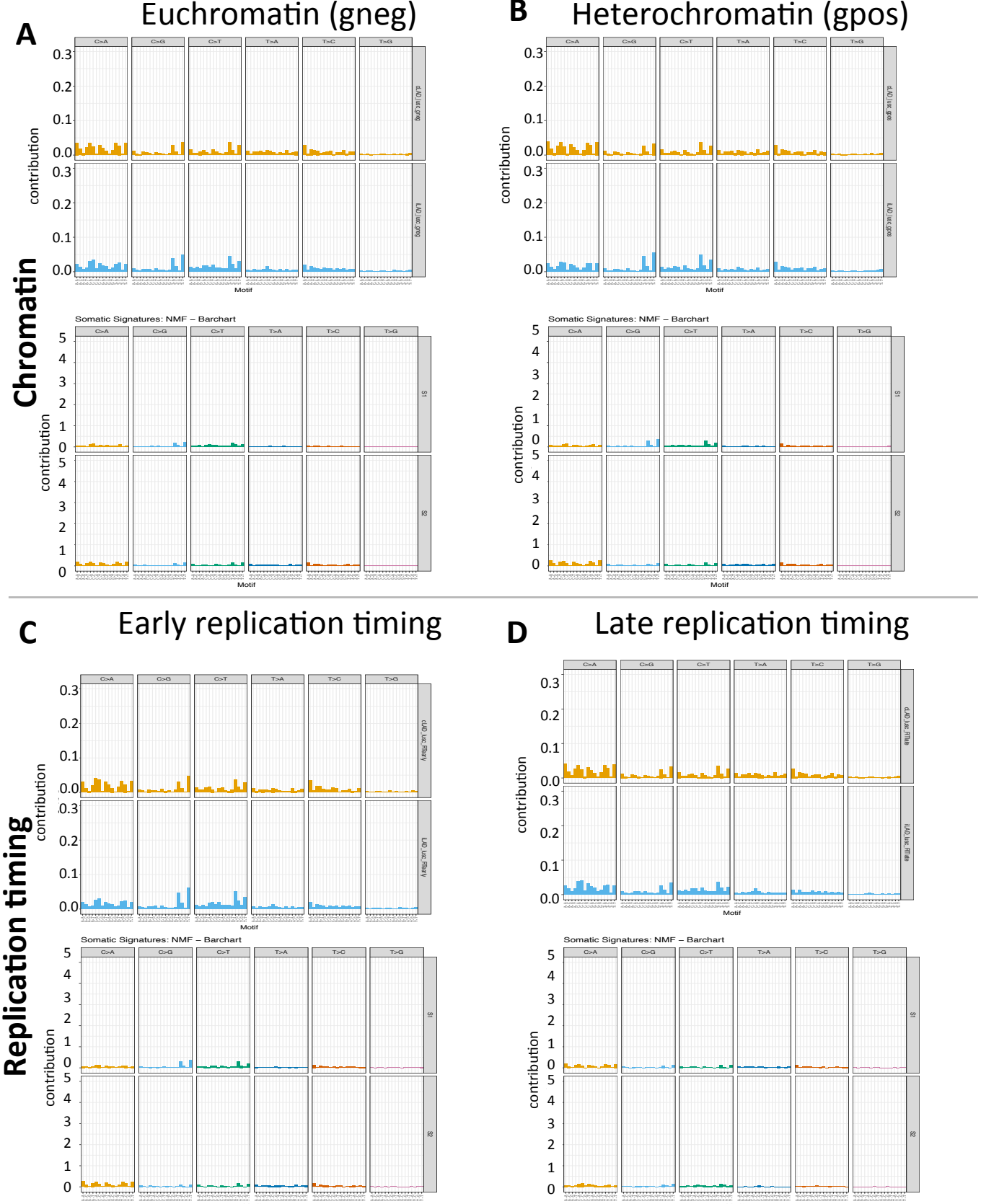

Comparing mutation signatures between nuclear core and periphery after adjusting for covariates in LUSC cohort. Somatic substitution patterns in their tri-nucleotide context (x-axis) and contribution (y-axis) of those substitution classes to the major mutation signatures in A) euchromatic (Giemsa-negative), B) heterochromatic (Giemsa-positive), C) constant early replicating, and D) constant late replication timing regions in the LUSC cohort. Order of the tri-nucleotide context is similar to that in Supplementary Figure 5. Plots were generated with the SomaticSignatures R package. Certain mutation signatures show variation depending on the nuclear context.

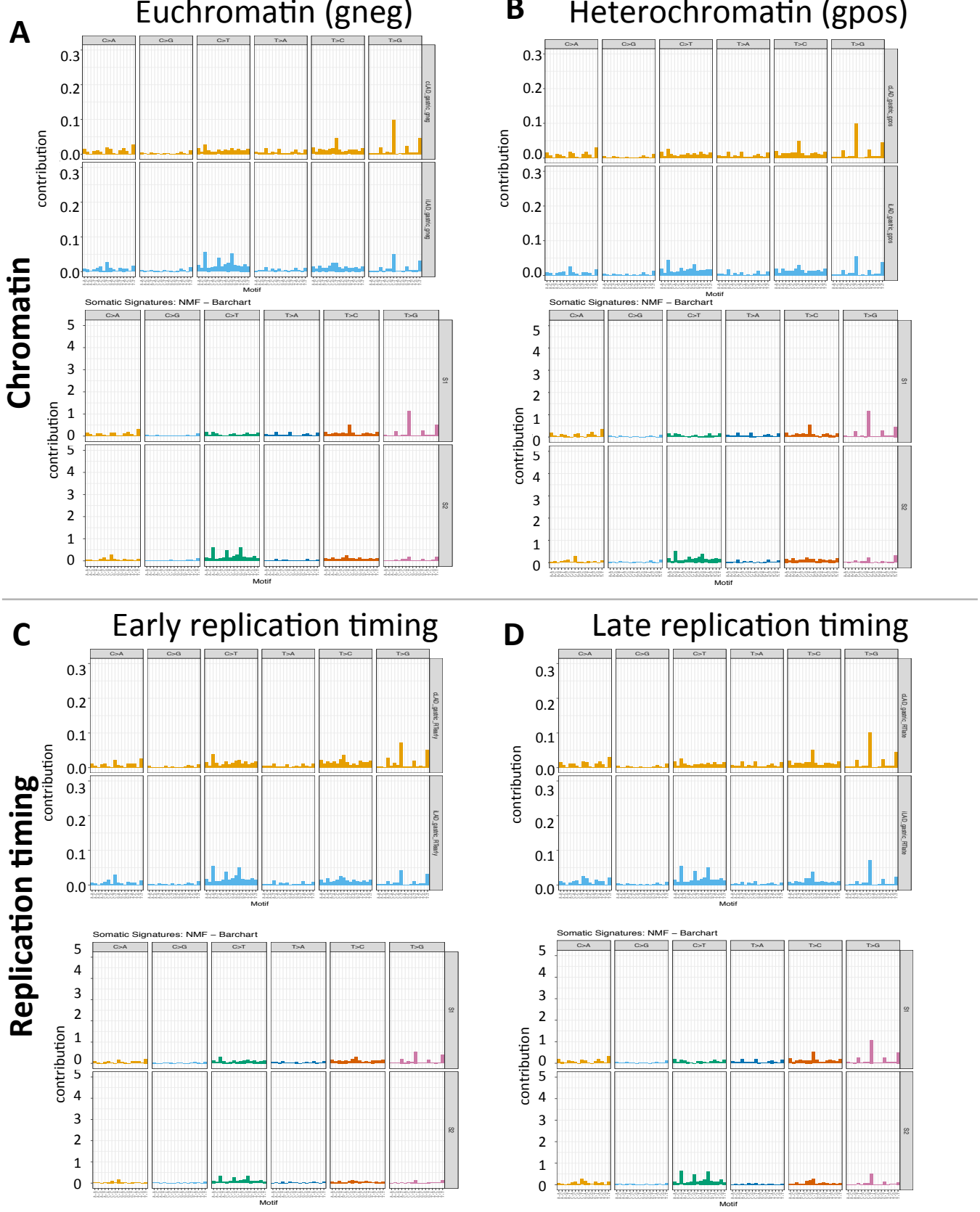

Comparing mutation signatures between nuclear core and periphery after adjusting for covariates in STAD cohort. Somatic substitution patterns in their tri-nucleotide context (x-axis) and contribution (y-axis) of those substitution classes to the major mutation signatures in A) euchromatic (Giemsa-negative), B) heterochromatic (Giemsa-positive), C) constant early replicating, and D) constant late replication timing regions in the STAD cohort. Order of the tri-nucleotide context is similar to that in Supplementary Figure 5. Plots were generated with the SomaticSignatures R package. Certain mutation signatures show variation depending on the nuclear context.

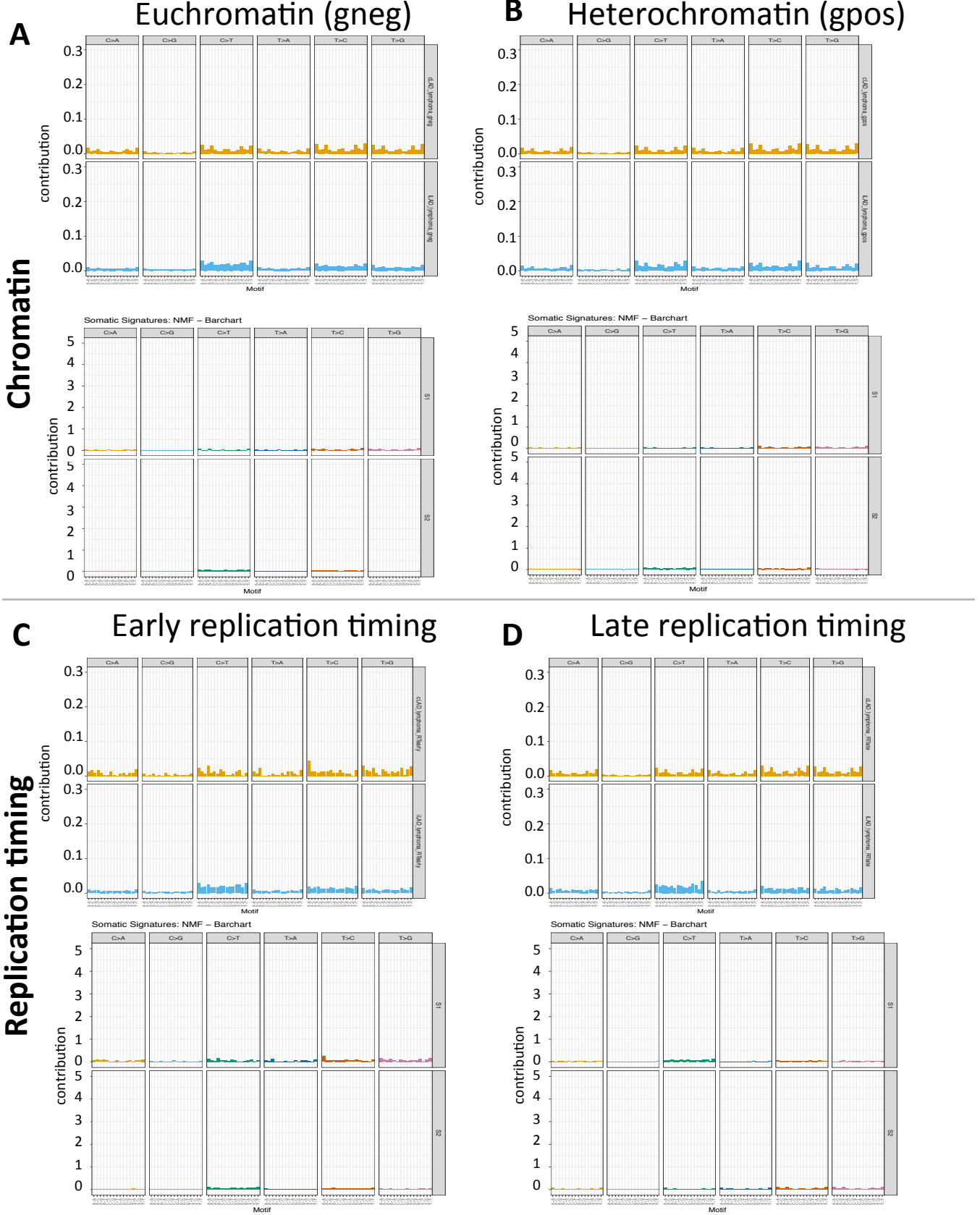

Comparing mutation signatures between nuclear core and periphery after adjusting for covariates in DLBCL cohort. Somatic substitution patterns in their tri-nucleotide context (x-axis) and contribution (y-axis) of those substitution classes to the major mutation signatures in A) euchromatic (Giemsa-negative), B) heterochromatic (Giemsa-positive), C) constant early replicating, and D) constant late replication timing regions in the DLBCL cohort. Order of the tri-nucleotide context is similar to that in Supplementary Figure 5. Plots were generated with the SomaticSignatures R package. Certain mutation signatures show variation depending on the nuclear context.

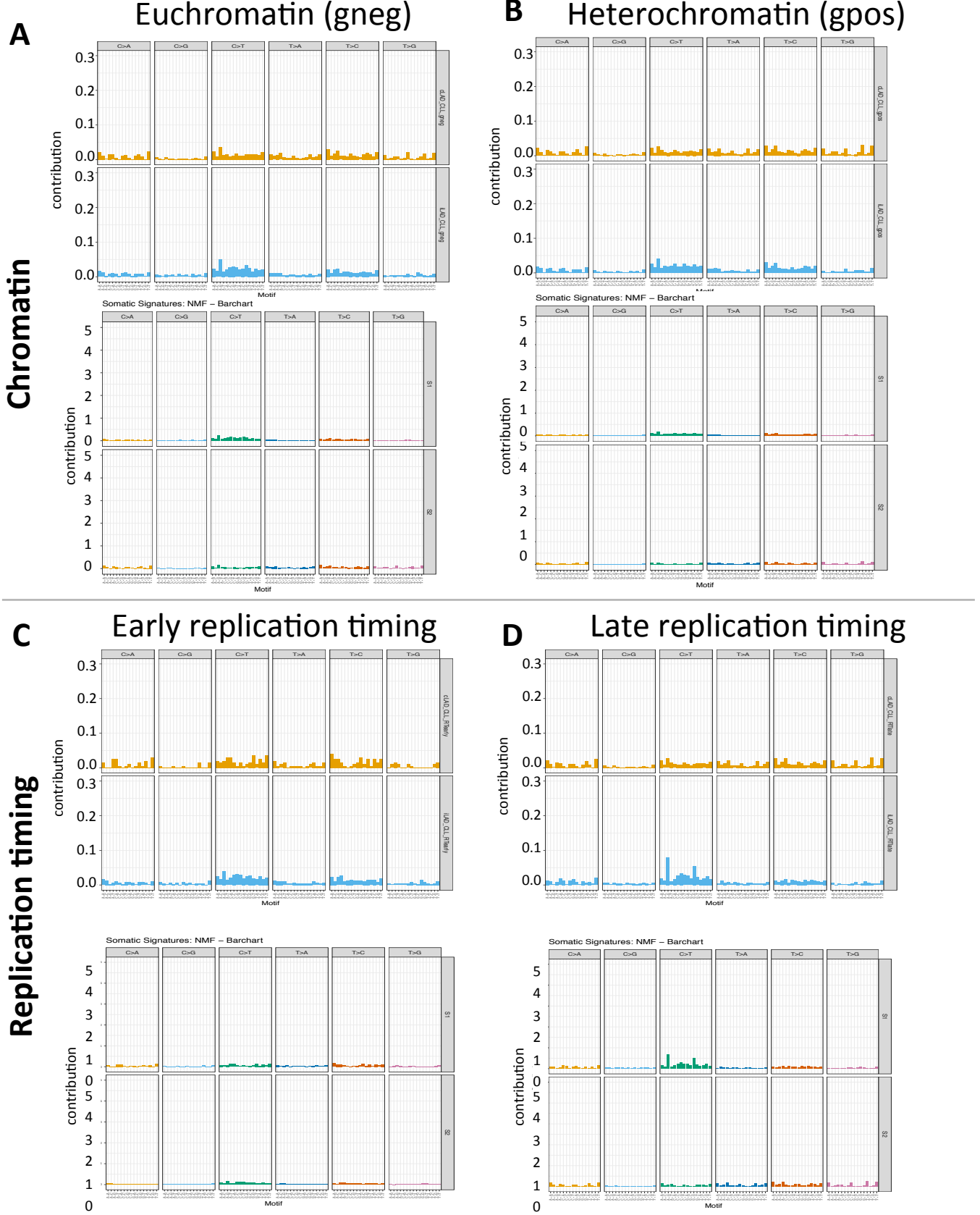

Comparing mutation signatures between nuclear core and periphery after adjusting for covariates in CLL cohort. Somatic substitution patterns in their tri-nucleotide context (x-axis) and contribution (y-axis) of those substitution classes to the major mutation signatures in A) euchromatic (Giemsa-negative), B) heterochromatic (Giemsa-positive), C) constant early replicating, and D) constant late replication timing regions in the CLL cohort. Order of the tri-nucleotide context is similar to that in Supplementary Figure 5. Plots were generated with the SomaticSignatures R package. Certain mutation signatures show variation depending on the nuclear context.

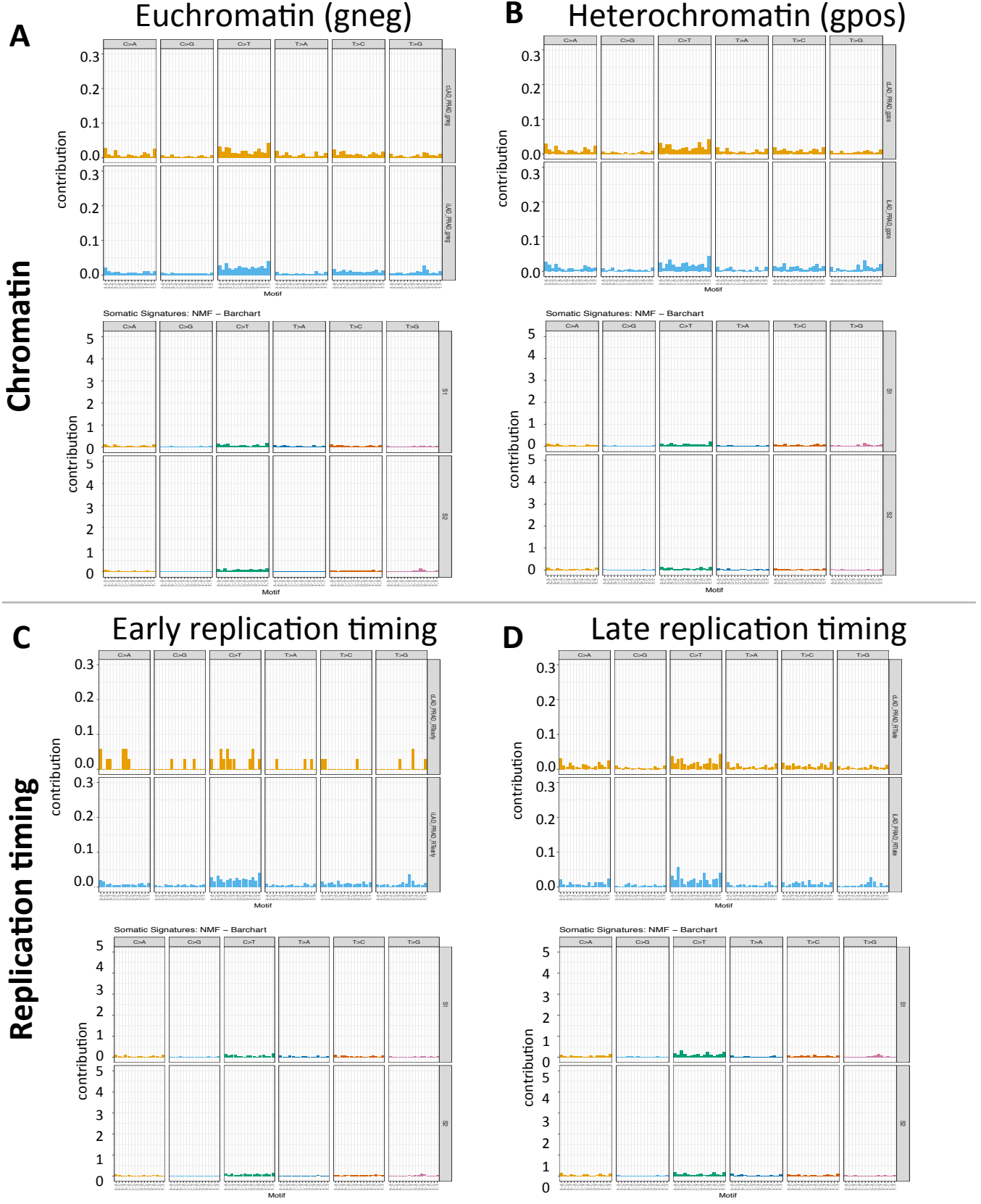

Comparing mutation signatures between nuclear core and periphery after adjusting for covariates in PRAD cohort. Somatic substitution patterns in their tri-nucleotide context (x-axis) and contribution (y-axis) of those substitution classes to the major mutation signatures in A) euchromatic (Giemsa-negative), B) heterochromatic (Giemsa-positive), C) constant early replicating, and D) constant late replication timing regions in the PRAD cohort. Order of the tri-nucleotide context is similar to that in Supplementary Figure 5. Plots were generated with the SomaticSignatures R package. Certain mutation signatures show variation depending on the nuclear context.

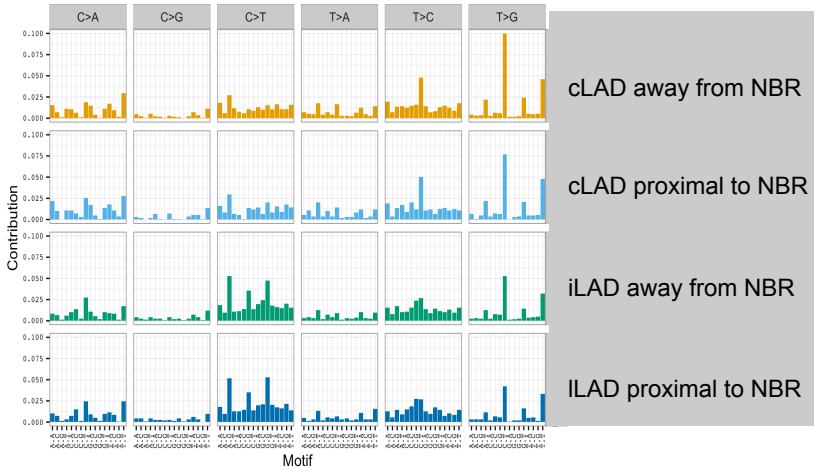

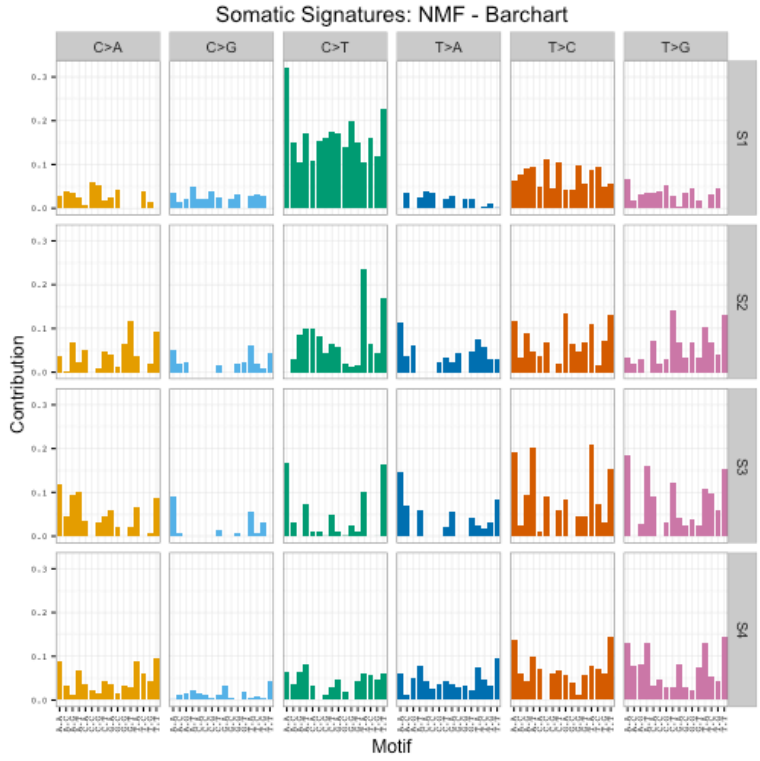

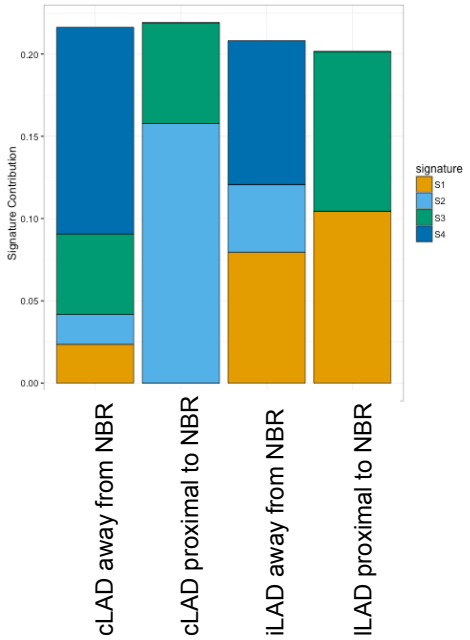

Mutation signatures between nuclear core and periphery after adjusting for proximity to nuclear pore in SKCA cohort.

Somatic substitution patterns (x-axis) and contribution (y-axis) of those substitution classes to the major mutation signatures in cLADs and iLADs proximal to and away from the Nup98-bound regions (NBRs) in the SKCA cohort. Plots were generated with the SomaticSignatures R package. Certain mutation signatures show variation depending on the nuclear context.

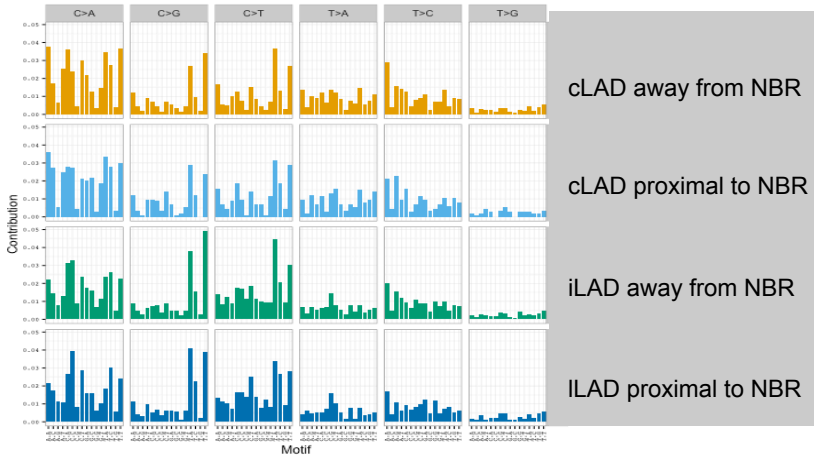

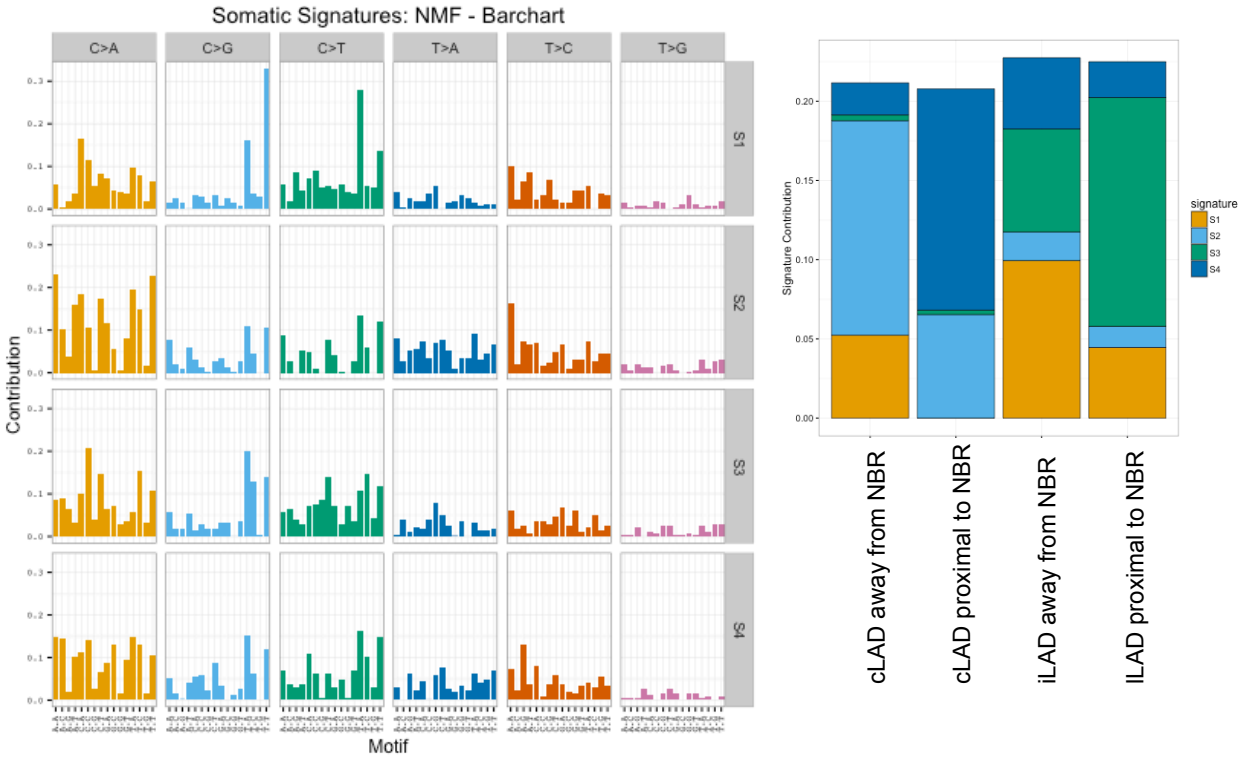

Mutation signatures between nuclear core and periphery after adjusting for proximity to nuclear pore in LUSC cohort.

Somatic substitution patterns (x-axis) and contribution (y-axis) of those substitution classes to the major mutation signatures in cLADs and iLADs proximal to and away from the Nup98-bound regions (NBRs) in the LUSC cohort. Plots were generated with the SomaticSignatures R package. Mutation signatures show some variation depending on the nuclear context.

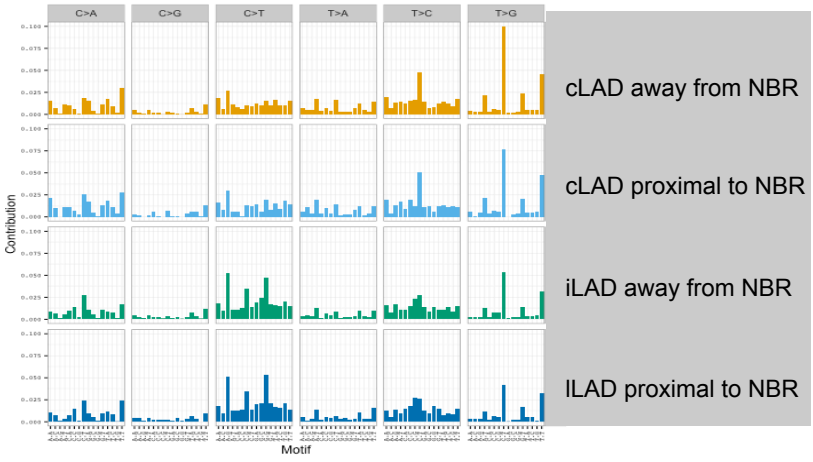

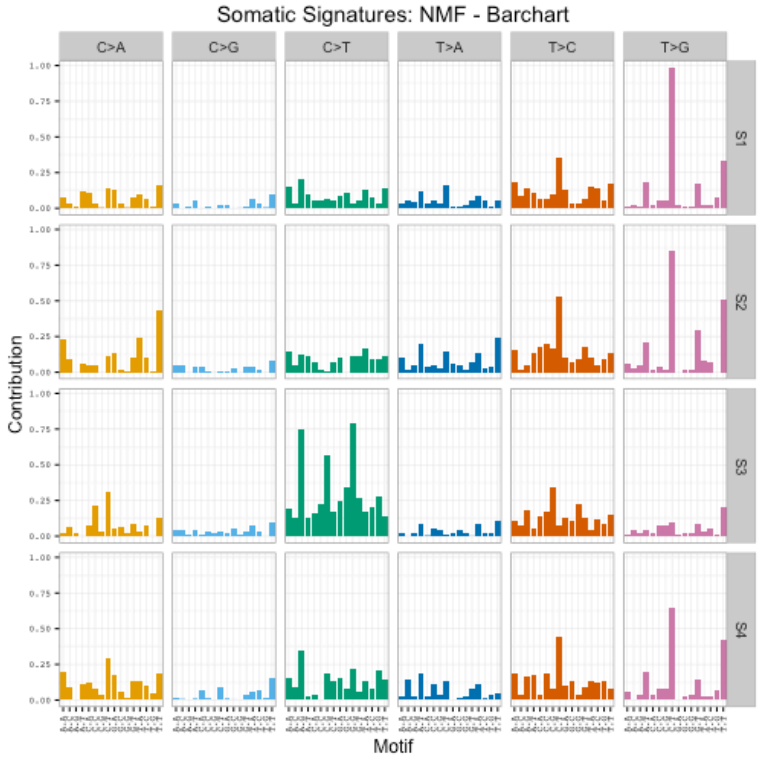

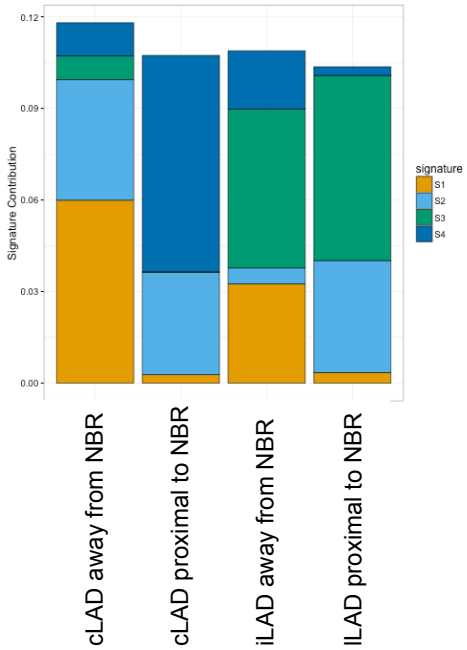

Mutation signatures between nuclear core and periphery after adjusting for proximity to nuclear pore in STAD cohort.

Somatic substitution patterns (x-axis) and contribution (y-axis) of those substitution classes to the major mutation signatures in cLADs and iLADs proximal to and away from the Nup98-bound regions (NBRs) in the STAD cohort. Plots were generated with the SomaticSignatures R package. Certain mutation signatures show variation depending on the nuclear context.

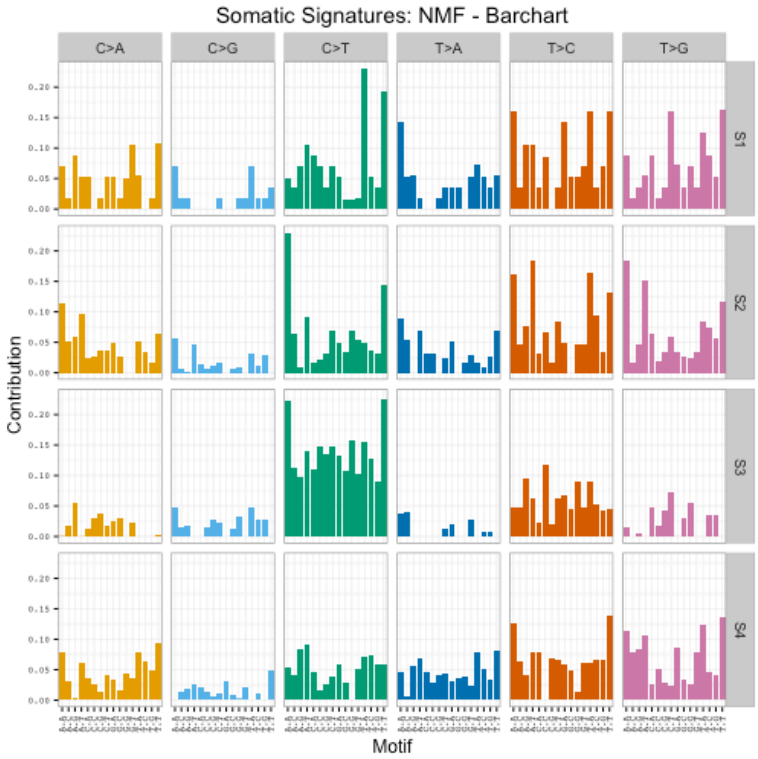

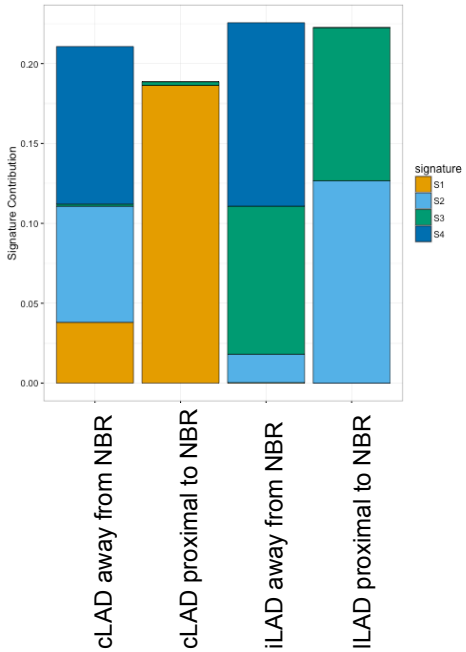

Mutation signatures between nuclear core and periphery after adjusting for proximity to nuclear pore in DLBCL cohort.

Somatic substitution patterns (x-axis) and contribution (y-axis) of those substitution classes to the major mutation signatures in cLADs and iLADs proximal to and away from the Nup98-bound regions (NBRs) in the DLBCL cohort. Plots were generated with the SomaticSignatures R package. Certain mutation signatures show variation depending on the nuclear context.

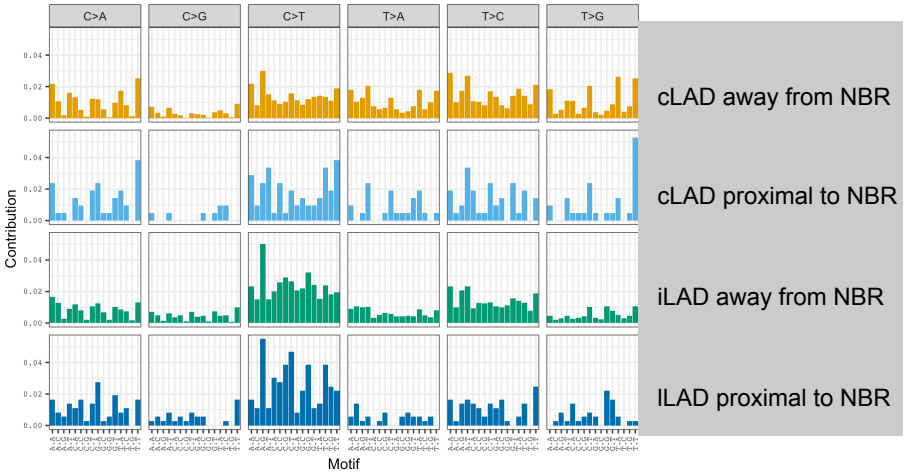

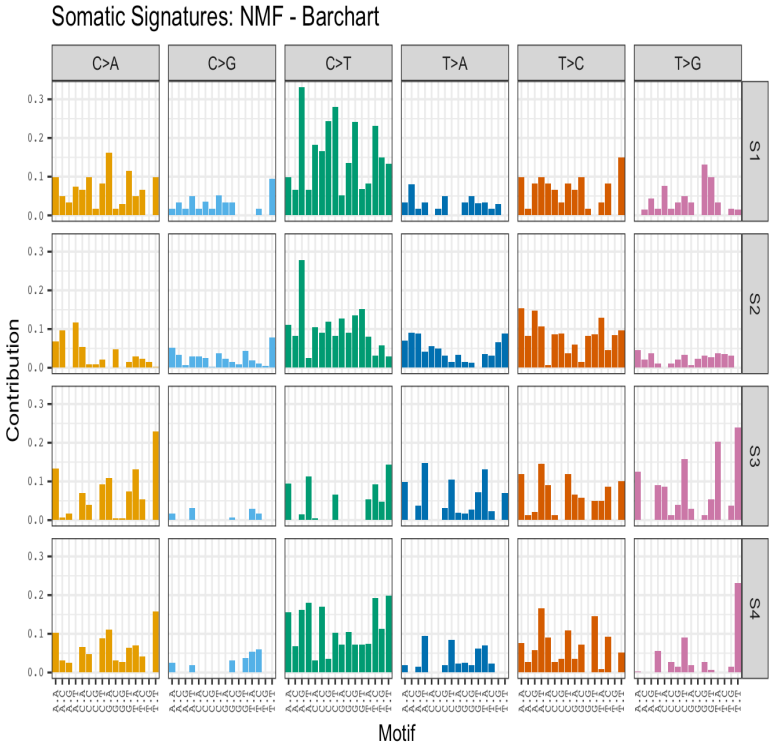

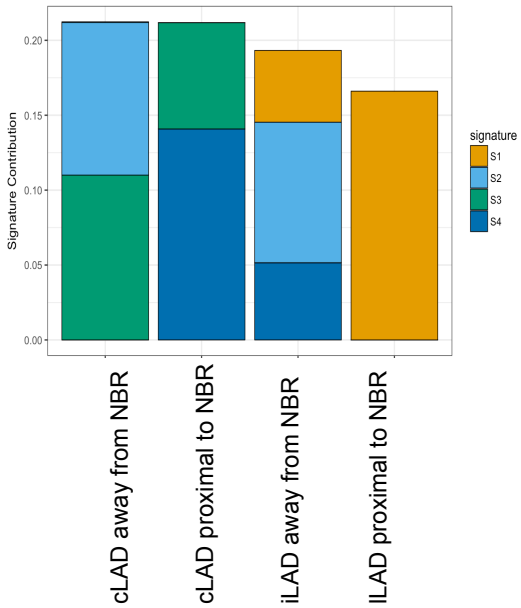

Mutation signatures between nuclear core and periphery after adjusting for proximity to nuclear pore in CLL cohort.

Somatic substitution patterns (x-axis) and contribution (y-axis) of those substitution classes to the major mutation signatures in cLADs and iLADs proximal to and away from the Nup98-bound regions (NBRs) in the CLL cohort. Plots were generated with the SomaticSignatures R package. Certain mutation signatures show variation depending on the nuclear context.

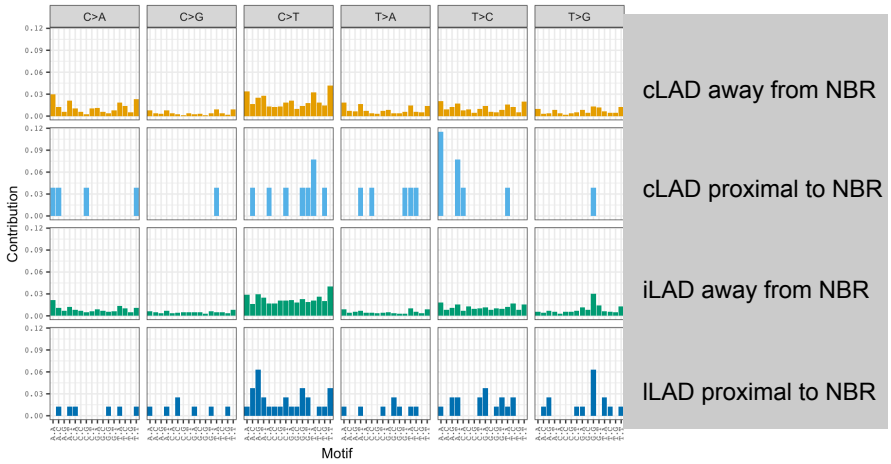

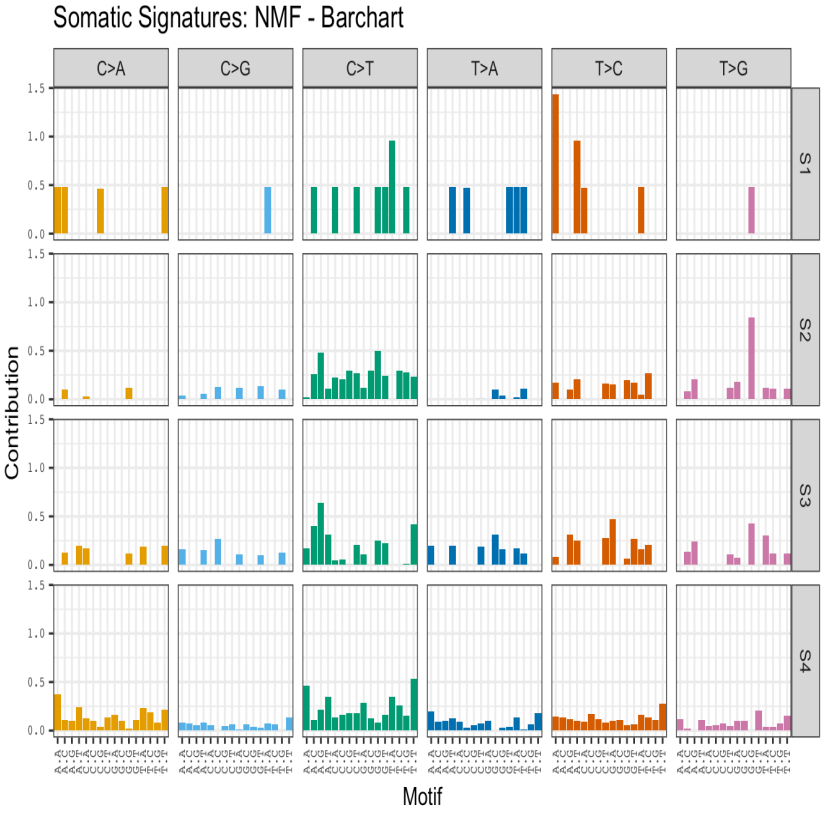

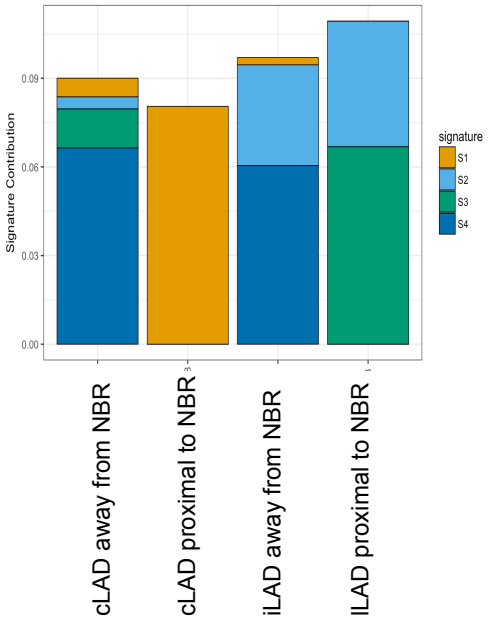

Mutation signatures between nuclear core and periphery after adjusting for proximity to nuclear pore in PRAD cohort.

Somatic substitution patterns (x-axis) and contribution (y-axis) of those substitution classes to the major mutation signatures in cLADs and iLADs proximal to and away from the Nup98-bound regions (NBRs) in the PRAD cohort. Plots were generated with the SomaticSignatures R package. Certain mutation signatures show variation depending on the nuclear context.